

Geostrophic balance preserving interpolation in mesh adaptive shallow-water ocean modelling

J. R. Maddison ^{a,*}, C. J. Cotter ^b, P. E. Farrell ^{c,d}

^a*Atmospheric, Oceanic and Planetary Physics, Department of Physics,
University of Oxford, Oxford, OX1 3PU, UK*

^b*Department of Aeronautics, Imperial College London, London, SW7 2AZ*

^c*Applied Modelling and Computation Group,
Department of Earth Science and Engineering,
Royal School of Mines,
Imperial College London, London, SW7 2AZ, UK*

^d*Institute of Shock Physics,
Royal School of Mines,
Imperial College London, London, SW7 2AZ, UK*

Abstract

The accurate representation of geostrophic balance is an essential requirement for numerical modelling of geophysical flows. Significant effort is often put into the selection of accurate or optimal balance representation by the discretisation of the fundamental equations. The issue of accurate balance representation is particularly challenging when applying dynamic mesh adaptivity, where there is potential for additional imbalance injection when interpolating to new, optimised meshes.

In the context of shallow-water modelling, we present a new method for preservation of geostrophic balance when applying dynamic mesh adaptivity. This approach is based upon interpolation of the Helmholtz decomposition of the Coriolis acceleration. We apply this in combination with a discretisation for which states in geostrophic balance are exactly steady solutions of the linearised equations on an f -plane; this method guarantees that a balanced and steady flow on a donor mesh remains balanced and steady after interpolation onto an arbitrary target mesh, to within machine precision. We further demonstrate the utility of this interpolant for states close to geostrophic balance, and show that it prevents pollution of the resulting solutions by imbalanced perturbations introduced by the interpolation.

Key words: Shallow-water equations; Finite element method; Discontinuous Galerkin, Geostrophic balance; Interpolation; Helmholtz decomposition

1 Introduction

It has been recognised in previous work on shallow-water modelling that the accurate representation of physical balance by the discrete system is of crucial importance. In Le Roux et al. (1998) a number of shallow-water finite element pairs are compared, and it is concluded that the majority of those tested are unable to represent physical balance accurately while simultaneously remaining free of spurious numerical modes. In Cotter et al. (2009b) a finite element pair is presented using a piecewise linear discontinuous element for velocity and a piecewise quadratic C^0 continuous element for layer thickness: the $P_{1\text{DG}}P_2$ finite element pair. This is shown to be free of spurious pressure modes (Cotter et al., 2009b,a) and, in Cotter et al. (2009a) in the context of shallow-water modelling, is shown to have the property that geostrophically balanced states with a constant stream function on the boundary are exactly steady solutions of the discrete linearised shallow-water equations on an f -plane. The $P_{1\text{DG}}P_2$ element pair is compared against a number of other low order discontinuous methods in Comblen et al. (2009), and found to be the most accurate choice amongst those tested. This discretisation is extended in Cotter et al. (2009b,a) to form a family of related $P_{(n-1)\text{DG}}P_n$ finite element pairs, all of which are free of pressure modes and exhibit this optimal balance property.

This paper is concerned with the application of dynamic mesh adaptivity to shallow-water ocean modelling. Dynamic mesh adaptivity allows the resolution of the computational mesh to be varied locally as a simulation develops, in order to resolve dynamically important regions of the flow and thereby increase the accuracy per degree of freedom of a model. While this has the potential for enabling numerical simulations of otherwise inaccessible systems, it presents an additional problem: as well as the possibility of imbalance injection in the numerical discretisation of the underlying equations, there is also a potential for imbalance injection by the mesh optimisation procedure itself.

Recently, dynamic mesh adaptive ocean modelling has been proposed by Pain et al. (2005); Piggott et al. (2008a). This approach utilises unstructured meshes in all three dimensions with dynamic mesh adaptivity applied using element-wise topological operations and nodal perturbations to optimise the mesh according to a metric derived from the interpolation error of simulation fields (Pain et al., 2001; Piggott et al., 2006; Munday et al., 2010). A feature of this approach is that, in each mesh adapt, the new optimised target mesh has, in general, no relationship to the original donor mesh, other than that each is some covering simplex partitioning of the same original domain. This generality presents a particularly challenging interpolation problem.

* Corresponding author

Email address: maddison@atm.ox.ac.uk (J. R. Maddison).

The Galerkin projection of fields between arbitrary two and three dimensional meshes is described in Farrell et al. (2009); Farrell (2009). This projection is (by definition) optimal in the least squares sense, and has the advantage that the integral of the projected field is exactly conserved. However, there is no guarantee that the projection injects no additional imbalance. In St-Cyr et al. (2008) statically refined mesh and uniform mesh simulations are compared in an adaptive mesh refinement (AMR) shallow-water model of a geostrophically balanced flow. It is noted that there is an increase in the error in the statically refined case, attributed to interpolation errors in the AMR ghost cells which “introduce slight disturbance” in this region, with the resulting errors growing faster in regions of stronger solution gradients. It is suggested that higher order schemes be used to mitigate this.

In this paper we seek to address the problem of imbalance injection by interpolation between arbitrary unstructured meshes. In the context of shallow-water modelling, we formulate an interpolant that, for the linearised system on an f -plane, guarantees that flows that are initially steady and in geostrophic balance remain steady and in balance after interpolation onto an arbitrary target mesh.

2 Formulation

In section 2.1 the finite element discretisation of the linearised shallow-water equations using the $P_{1DG}P_2$ finite element pair is outlined. A set of properties for geostrophic balance preserving interpolants is presented in section 2.2 for which, for the linearised system on an f -plane, an initially steady and geostrophically balanced state remains steady and balanced after interpolation onto an arbitrary target mesh. An interpolant satisfying these properties is given in section 2.3

2.1 Discretised shallow-water equations

The linearised shallow-water equations with free slip boundary conditions are:

$$\frac{\partial \mathbf{u}}{\partial t} + f \hat{\mathbf{z}} \times \mathbf{u} + g \nabla \eta = 0, \quad (1a)$$

$$\frac{\partial \eta}{\partial t} + H \nabla \cdot \mathbf{u} = 0, \quad (1b)$$

$$\mathbf{u} \cdot \hat{\mathbf{n}} = 0 \text{ on } \partial\Omega, \quad (1c)$$

where \mathbf{u} is the (horizontal) velocity, H is the mean layer thickness, η is the deviation of the layer thickness from H , f is the Coriolis parameter, g is the gravitational acceleration and $\hat{\mathbf{n}}$ is a unit normal on the boundary $\partial\Omega$. From this one may define two non-dimensional parameters: the Rossby number $Ro = U/fD$ and the Froude number $Fr = \sqrt{U/gH}$, where U and D are characteristic flow speeds and spatial scales respectively.

Multiplying equations (1a) and (1b) by test functions \mathbf{w} and ϕ respectively, integrating over the domain Ω , integrating by parts and applying the free slip boundary condition yields the weak form:

$$\int_{\Omega} \mathbf{w} \frac{\partial \mathbf{u}}{\partial t} + f \mathbf{w} \cdot (\hat{\mathbf{z}} \times \mathbf{u}) + g \mathbf{w} \cdot \nabla \eta = 0 \quad \forall \mathbf{w}, \quad (2a)$$

$$\int_{\Omega} \phi \frac{\partial \eta}{\partial t} - H \int_{\Omega} \nabla \phi \cdot \mathbf{u} = 0 \quad \forall \phi. \quad (2b)$$

Choosing some simplex covering partition of Ω (the mesh), restricting \mathbf{w} and \mathbf{u} to be piecewise linear discontinuous and restricting ϕ and η to be piecewise quadratic C^0 continuous completes the $P_{1DG}P_2$ spatial discretisation:

$$\int_{\Omega} \mathbf{w}^{\delta} \frac{d\mathbf{u}^{\delta}}{dt} + f \mathbf{w}^{\delta} \cdot (\hat{\mathbf{z}} \times \mathbf{u}^{\delta}) + g \mathbf{w}^{\delta} \cdot \nabla \eta^{\delta} = 0 \quad \forall \mathbf{w}^{\delta}, \quad (3a)$$

$$\int_{\Omega} \phi^{\delta} \frac{d\eta^{\delta}}{dt} - H \int_{\Omega} \nabla \phi^{\delta} \cdot \mathbf{u}^{\delta} = 0 \quad \forall \phi^{\delta}, \quad (3b)$$

where ζ^{δ} denotes the finite element approximation for ζ . Introducing basis function expansions of \mathbf{w}^{δ} , \mathbf{u}^{δ} , ϕ^{δ} and η^{δ} , this can be re-expressed as:

$$\frac{d}{dt} M_1 \tilde{\mathbf{u}} + f L \tilde{\mathbf{u}} + g C \tilde{\eta} = 0, \quad (4a)$$

$$\frac{d}{dt} M_2 \tilde{\eta} - H C^T \tilde{\mathbf{u}} = 0, \quad (4b)$$

where $\tilde{\mathbf{u}}$ and $\tilde{\eta}$ are the nodal values for velocity and layer thickness respectively and:

$$\begin{aligned}
M_1 &= \text{diag}(M'_1, M'_1), & M_2 &= \text{diag}(M'_2, M'_2), \\
L &= \begin{pmatrix} 0 & -1 \\ 1 & 0 \end{pmatrix} M'_1, & C_T &= (C^x, C^y).
\end{aligned} \tag{5}$$

M'_1 and M'_2 are the velocity space and layer thickness space mass matrices respectively, and C^T is the discrete divergence matrix:

$$\begin{aligned}
(M'_1)_{ij} &= \int_{\Omega} \psi_i \psi_j, & (M'_2)_{ij} &= \int_{\Omega} \xi_i \xi_j, \\
(C^q)_{ij} &= \int_{\Omega} \frac{\partial \xi_i}{\partial q} \psi_j \quad q \in \{x, y\},
\end{aligned} \tag{6}$$

where the ψ_i and ξ_i are the $P_{1\text{DG}}$ and P_2 elemental basis functions respectively. Choosing some time discretisation allows equations (4a) and (4b) to be integrated on a computer.

2.2 Geostrophic balance preserving interpolants

Consider interpolation between a donor mesh A and a target mesh B . Let $(\dots)^A$ and $(\dots)^B$ denote ‘‘on donor’’ and ‘‘on target’’ respectively - for example $(C^T)^A$ and $(C^T)^B$ are the divergence matrices, as per (6), assembled on the donor and target meshes respectively. Consider an interpolation procedure as follows:

- (1) Perform a Helmholtz decomposition of the Coriolis acceleration $\mathbf{F}_*^A = f \hat{\mathbf{z}} \times \tilde{\mathbf{u}}^A$ on the donor mesh:

$$M_1^A \mathbf{F}^A = M_1^A \mathbf{F}_*^A + C^A \Phi^A, \tag{7}$$

for some scalar potential Φ^A and discrete divergence free \mathbf{F}^A .

- (2) Interpolate \mathbf{F}^A , Φ^A and $\tilde{\eta}^A$ from the donor to the target to form \mathbf{F}^B , Φ^B and $\tilde{\eta}^B$, using interpolants with the following properties:

$$(M_1^A)^{-1} C^A \Phi^A \times \hat{\mathbf{n}} = 0 \text{ on } \partial\Omega \Rightarrow (M_1^B)^{-1} C^B \Phi^B \times \hat{\mathbf{n}} = 0 \text{ on } \partial\Omega, \tag{8a}$$

$$\mathbf{F}^A = 0 \Rightarrow \mathbf{F}^B = 0, \tag{8b}$$

$$\Phi^A = g \tilde{\eta}^A \Rightarrow \Phi^B = g \tilde{\eta}^B. \tag{8c}$$

(3) Recompose \mathbf{F}_*^B from Φ^B and \mathbf{F}^B :

$$M_1^B \mathbf{F}_*^B = M_1^B \mathbf{F}^B - C^B \Phi^B. \quad (9)$$

The Helmholtz decomposition splits the Coriolis acceleration into a curl-free scalar potential gradient component and a divergence free residual (Weyl, 1940; Ladyzhenskaya, 1969). Only the scalar potential gradient component can be cancelled from equation (4a) by a layer thickness gradient. For incompressible Navier-Stokes, this scalar potential gradient component must be exactly cancelled by the pressure gradient, with the diagnostic pressure field acting as a Lagrange multiplier via which the incompressibility constraint is applied.

Property (8b) states the somewhat trivial requirement that zero is preserved by the interpolant for \mathbf{F} . Property (8c) couples the velocity and layer thickness interpolation, and can be achieved if Φ and $\tilde{\eta}$ use the same interpolant and that interpolant is scale invariant. Property (8a) asserts that the interpolant for Φ preserves zero tangential gradients on the domain boundary, and is required in order to avoid generation of grid scale boundary Kelvin waves by the interpolation.

We now proceed to prove that this interpolant, when applied to a $P_{\text{IDG}}P_2$ discretisation of the linearised shallow-water equations on an f -plane, guarantees that a steady and geostrophically balanced state on the donor mesh results in a state that is steady and balanced on the target mesh. By definition, for a geostrophically balanced state on the donor:

$$fL^A \tilde{\mathbf{u}}^A = -gC^A \tilde{\eta}^A. \quad (10)$$

By equation (7) $\mathbf{F}^A = 0$ and $\Phi^A = g\tilde{\eta}^A$, and hence by properties (8b) and (8c) $\mathbf{F}^B = 0$ and $\Phi^B = g\tilde{\eta}^B$. Hence, by equation (9), on the target:

$$fL^B \tilde{\mathbf{u}}^B = -gC^B \tilde{\eta}^B. \quad (11)$$

Also, since \mathbf{F}_* is perpendicular to $\tilde{\mathbf{u}}$:

$$\begin{aligned}
\tilde{\mathbf{u}}^A \cdot \hat{\mathbf{n}} = 0 \text{ on } \partial\Omega &\Rightarrow \mathbf{F}_*^A \times \hat{\mathbf{n}} = 0 \text{ on } \partial\Omega \\
&\Rightarrow (M_1^A)^{-1} C^A \Phi^A \times \hat{\mathbf{n}} = 0 \text{ on } \partial\Omega && \text{by (10)} \\
&\Rightarrow (M_1^B)^{-1} C^B \Phi^B \times \hat{\mathbf{n}} = 0 \text{ on } \partial\Omega && \text{by (8a)} \\
&\Rightarrow \mathbf{F}_*^B \times \hat{\mathbf{n}} = 0 \text{ on } \partial\Omega \\
&\Rightarrow \tilde{\mathbf{u}}^B \cdot \hat{\mathbf{n}} = 0 \text{ on } \partial\Omega. && (12)
\end{aligned}$$

From (Cotter et al., 2009a), if using the $P_{1\text{DG}}P_2$ element pair on an f -plane:

$$\begin{aligned}
fL\tilde{\mathbf{u}} + gC\tilde{\eta} = 0 \text{ and } \tilde{\mathbf{u}} \cdot \hat{\mathbf{n}} = 0 \text{ on } \partial\Omega \\
\Leftrightarrow \frac{\partial \tilde{\mathbf{u}}}{\partial t} = 0 \text{ and } \frac{\partial \tilde{\eta}}{\partial t} = 0. && (13)
\end{aligned}$$

Hence by (11), (12) and (13) the solution on the target mesh is geostrophically balanced and exactly steady.

2.3 Implementation and boundary conditions

The Helmholtz decomposition of the Coriolis acceleration on the donor mesh is equivalent to the pressure projection method commonly used for incompressible Navier-Stokes solvers (Chorin, 1967; Temam, 1968; Gresho, 1990). Multiplying equation (7) by $(C^T)^A(M_1^A)^{-1}$ and using $C^T \mathbf{F}^A = 0$ leads to the elliptic equation:

$$(C^T)^A(M_1^A)^{-1}C^A\Phi^A = -(C^T)^A\mathbf{F}_*^A. \quad (14)$$

Note that here the consistent mass matrix can be used as the $P_{1\text{DG}}$ mass matrix M_1^A is block diagonal, and hence the Laplacian matrix $(C^T)^A(M_1^A)^{-1}C^A$ is sparse. From this Φ^A and \mathbf{F}^A can be determined. Following interpolation of the Helmholtz decomposition \mathbf{F}_*^B can be diagnosed directly from Φ^B and \mathbf{F}^B via equation (9). Therefore, the key step in forming a geostrophic balance preserving interpolant is to choose interpolants for Φ , $\tilde{\eta}$ and \mathbf{F} such that the properties (8a), (8b) and (8c) are satisfied.

One simple approach is to apply a Galerkin projection of \mathbf{F} from the donor mesh to the target mesh, as described in Farrell et al. (2009), and to interpolate Φ and $\tilde{\eta}$ using collocation: evaluation of the donor fields at the nodal coordinates of the target mesh. Since

Galerkin projection and collocation are linear, properties (8b) and (8c) are satisfied. Collocation also preserves constant boundary values, and hence property (8a) is satisfied. However, collocation (at least for piecewise linear fields) erodes solutions bounds and has no optimality properties (Farrell, 2009).

A more accurate approach is to apply a mesh-to-mesh Galerkin projection of Φ and $\tilde{\eta}$. This does not in general satisfy property (8a), although this issue can be resolved by using a further decomposition of Φ , with an equivalent decomposition of $\tilde{\eta}$ in order to satisfy property (8c). Assuming Ω is simply connected, Φ^A can be decomposed into:

$$\Phi^A = \Phi_C^A + \Phi_R^A, \quad (15)$$

where Φ_C^A is equal to some constant c on the boundary, and Φ_R^A is some residual. Φ_C^A can be re-expressed:

$$\Phi_C^A = \Phi_0^A + c\Phi_1. \quad (16)$$

Here Φ_0 and Φ_1 satisfy:

$$N_0^A \Phi_0^A = N^A \Phi^A, \quad (17a)$$

$$N_1^A \Phi_1^A = 0, \quad (17b)$$

where N^A is the discrete Laplacian matrix $N^A = (C^T)^A (M_1^A)^{-1} C^A$, N_0^A is N^A with a Dirichlet boundary condition of zero on $\partial\Omega$ and N_1^A is N^A with a Dirichlet boundary condition of one on $\partial\Omega$. Minimising $\|\Phi_R^A\|_{L^2}$ subject to (15) then yields a unique value for c :

$$c = \frac{\langle \Phi_1^A, \Phi^A - \Phi_0^A \rangle_{L^2}}{\langle \Phi_1^A, \Phi_1^A \rangle_{L^2}}. \quad (18)$$

This choice of c has the property that if Φ^A is constant on $\partial\Omega$, then $\Phi_R^A = 0$. Applying a Galerkin projection of Φ_C^A and Φ_R^A from the donor mesh to the target mesh, with a Dirichlet boundary condition of c on $\partial\Omega$ for Φ_C^A , therefore guarantees that the boundary property (8a) is satisfied.

Note that using the mass matrix in place of the Laplacian matrix, $N^A = M_2^A$, is not suitable here, as this results in non-smooth Φ_C^A and Φ_R^A , with strong gradients close

to the boundary which can generate significant noise in the donor-to-target Galerkin projection.

The full geostrophic balance preserving interpolation procedure is therefore:

- (1) Compute \mathbf{F}_*^A from $\tilde{\mathbf{u}}^A$.
- (2) Solve equation (14) for Φ^A and compute \mathbf{F}^A using equation (7).
- (3) Solve equations (17a) and (17b), with $N^A = (\mathbf{C}^T)^A (\mathbf{M}_1^A)^{-1} \mathbf{C}^A$, for Φ_0^A and Φ_1^A , and compute Φ_C^A and Φ_R^A . Perform a similar decomposition for $\tilde{\eta}^A$ to form $\tilde{\eta}_C^A$ and $\tilde{\eta}_R^A$.
- (4) Apply a Galerkin projection from the donor mesh to the target mesh of Φ_C^A , Φ_R^A , $\tilde{\eta}_C^A$, $\tilde{\eta}_R^A$ and \mathbf{F}^A , with Dirichlet boundary conditions for Φ_C^A and $\tilde{\eta}_C^A$ as determined from equation (18), to form Φ_C^B , Φ_R^B , $\tilde{\eta}_C^B$, $\tilde{\eta}_R^B$ and \mathbf{F}^B .
- (5) Compute Φ^B from Φ_C^B and Φ_R^B using equation (15). Similarly compute $\tilde{\eta}^B$ from $\tilde{\eta}_C^B$ and $\tilde{\eta}_R^B$.
- (6) Compute \mathbf{F}_*^B using equation (9).
- (7) Compute $\tilde{\mathbf{u}}^B$ from \mathbf{F}_*^B .

3 Numerical Examples

In this section several numerical examples of geostrophic balance preservation using the interpolation procedure presented above are given. In section 3.1 it is demonstrated that the geostrophic balance preserving interpolant ensures that a steady and balanced state remains steady and balanced after interpolation. In section 3.2 a state close to geostrophic balance is considered, and it is shown that the geostrophic balance preserving interpolant avoids imbalance injection. The interpolant is applied to a Kelvin wave in section 3.3, and the accuracy of the interpolant in the L_2 norm is quantified in section 3.4.

3.1 Preservation of balance

The $P_{1DG}P_2$ linearised shallow-water equations (4a) and (4b) on an f -plane were discretised in time using Crank-Nicolson finite differencing (Crank and Nicolson, 1947), and the linear systems solved with preconditioned conjugate gradients using the PETSc library (Balay et al., 1997, 2008, 2009). Further details of the discretisation are given in Cotter et al. (2009a).

In order to test for imbalance injection by mesh-to-mesh interpolation, two pseudo-isotropic circular meshes A and B were generated using Gmsh (Geuzaine and Remacle,

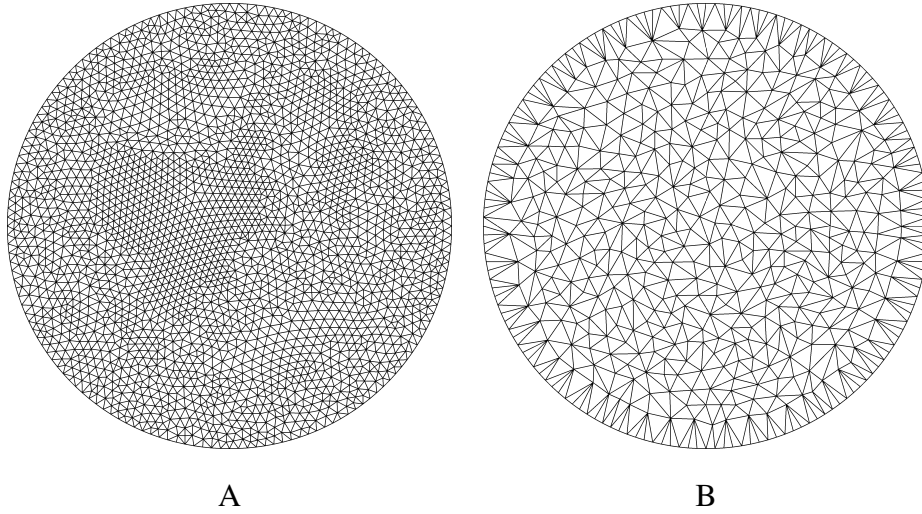


Fig. 1. Pseudo-isotropic meshes used to test for imbalance injection by mesh-to-mesh interpolation. Mesh B has one half the resolution of mesh A.

2009) and the ani2d mesh optimisation library (Vasilevskii and Lipnikov, 1999; Agouzal et al., 1999), with mesh A of one half the resolution of mesh B, as shown in figure 1. Meshes A and B have 2447 and 557 nodes respectively. Following the balance preservation test of Le Roux et al. (1998); Cotter et al. (2009b), the system was initialised on mesh A with a Gaussian profile for layer thickness, shown in figure 2, and with a velocity field initialised so as to be in discrete geostrophic balance with that profile as per equation (10). The solution was then interpolated backwards and forwards between meshes A and B at ten timestep intervals. Since geostrophically balanced states with a constant stream function on the boundary are known to be exactly steady when using the $P_{1DG}P_2$ element pair (Cotter et al., 2009a), any transience observed in the simulation is purely due to imbalance injection by the interpolation procedure.

The model was integrated for 210 timesteps of $6 \times 10^{-4}(D/U)$ at Rossby number 0.06 and Froude number 0.07 for a total of 20 interpolations between meshes A and B. Three interpolants were tested: a first order accurate interpolant as proposed by Grandy (1999) for both velocity and layer thickness (“Grandy interpolation”), Galerkin projection for velocity and layer thickness, and the geostrophic balance preserving interpolant presented in the previous section. Collocation was not tested, as this is not well defined at element boundaries and hence is unsuitable for use with the discontinuous velocity field.

The final layer thickness and change in layer thickness from the initial condition are shown in figure 3, and the maximum change in layer thickness between each interpolation is shown in figure 4. Grandy interpolation is observed to inject imbalance everywhere after each interpolation, resulting in a severe degradation of the simulation fields

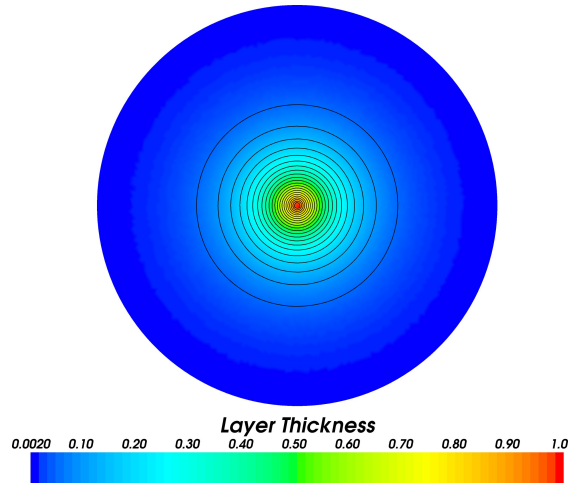


Fig. 2. Gaussian profile layer thickness used as an initial condition for the geostrophic balance preservation test.

after just a single interpolation. Galerkin projection is observed to inject imbalance towards the centre of the domain, near the layer thickness maximum. The resulting gravity waves propagate outwards polluting the global solution, and accumulate after every interpolation. The geostrophic balance preserving interpolant is exactly steady, to within machine precision, after every interpolation, with a change in layer thickness between interpolations of $\lesssim 10^{-13}$. The residual imbalance between interpolations is attributed to double precision round-off error.

After 20 interpolations the L_2 layer thickness error is 20% (of initial layer thickness L_2 norm) for Grandy interpolation, 2.7% for Galerkin projection and 2.0% for the geostrophic balance preserving interpolant. While Galerkin projection is optimal in the L_2 norm for each interpolation, the imbalance injection and resulting pollution of the solution by gravity waves leads to a reduced accuracy in the L_2 norm of the final model solution with respect to the geostrophic balance preserving interpolant.

To further demonstrate geostrophic balance preservation the test was repeated on two anisotropic circular meshes C and D generated using Gmsh (Geuzaine and Remacle, 2009) and the ani2d mesh optimisation library (Vasilevskii and Lipnikov, 1999; Agouzal et al., 1999) with elements stretched in perpendicular directions as shown in figure 5. Meshes C and D have 7986 and 7205 nodes respectively, and a maximum element edge length ratio of ~ 30 . The velocity field was initialised to be in discrete geostrophic balance with this layer thickness as before, with interpolations backwards and forwards between the two meshes at 10 timestep intervals for 20 interpolations. Simulations were conducted using the geostrophic balance preserving interpolant, Galerkin projection, and Grandy interpolation, with the change in layer thickness between interpolations

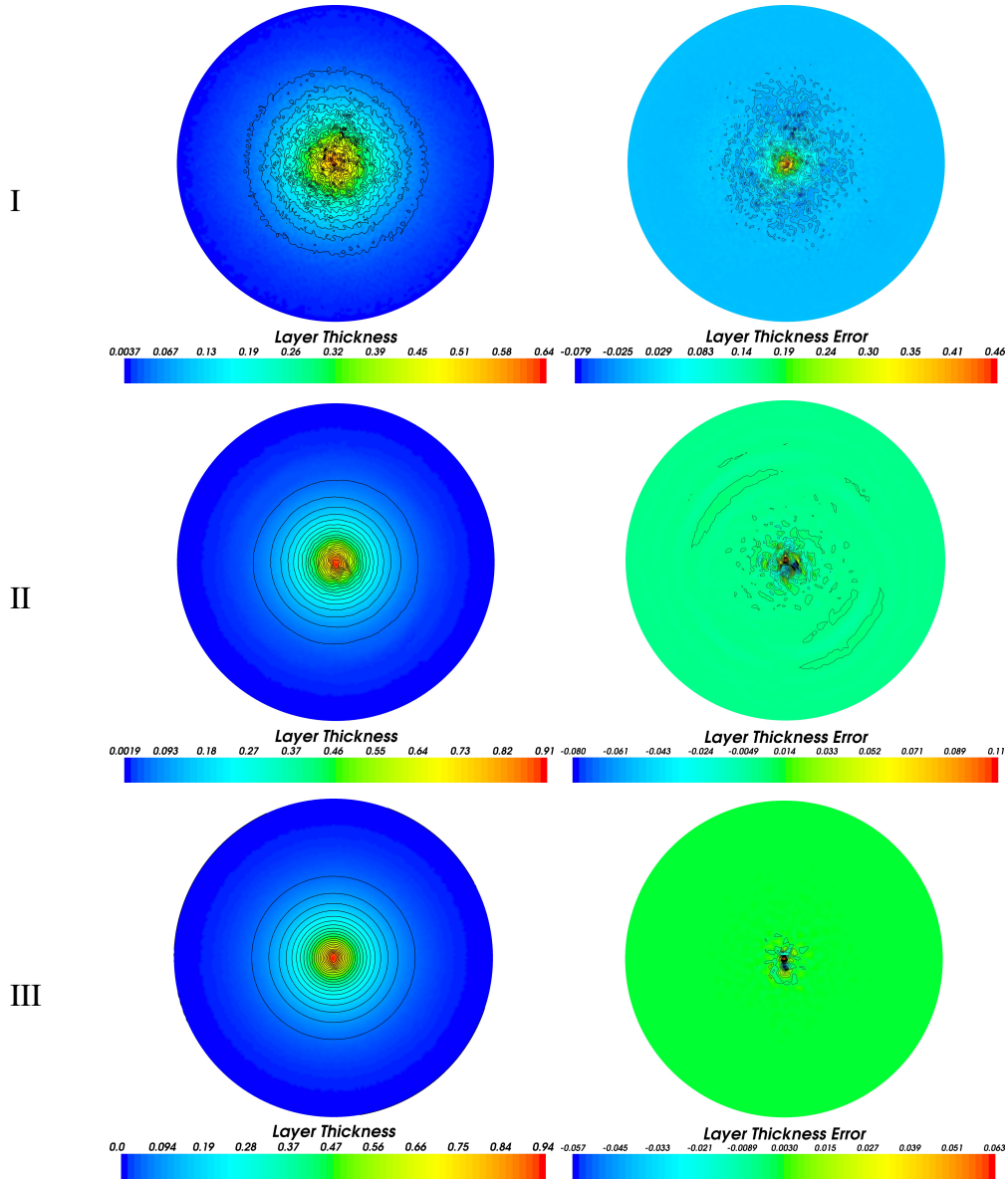


Fig. 3. The final solution of the geostrophic balance preservation test after 20 repeated interpolations backwards and forwards between the pseudo-isotropic meshes A and B in figure 1. Left: Final layer thickness. Right: Change in layer thickness from the initial condition in figure 2. I: Grandy interpolation. II: Galerkin projection. III: Helmholtz decomposed geostrophic balance preserving interpolation.

shown in figure 6. When applying the geostrophic balance preserving interpolation the maximum change between interpolations was $\lesssim 10^{-13}$ as before.

Finally, the geostrophic balance preservation the test was repeated using the anisotropic

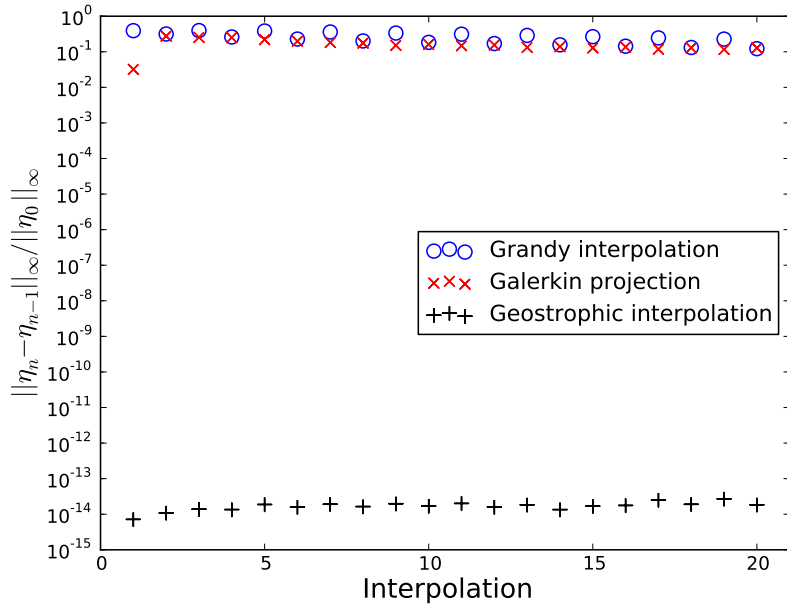


Fig. 4. The maximum change in layer thickness between interpolations backwards and forwards between the pseudo-isotropic meshes A and B in figure 1.

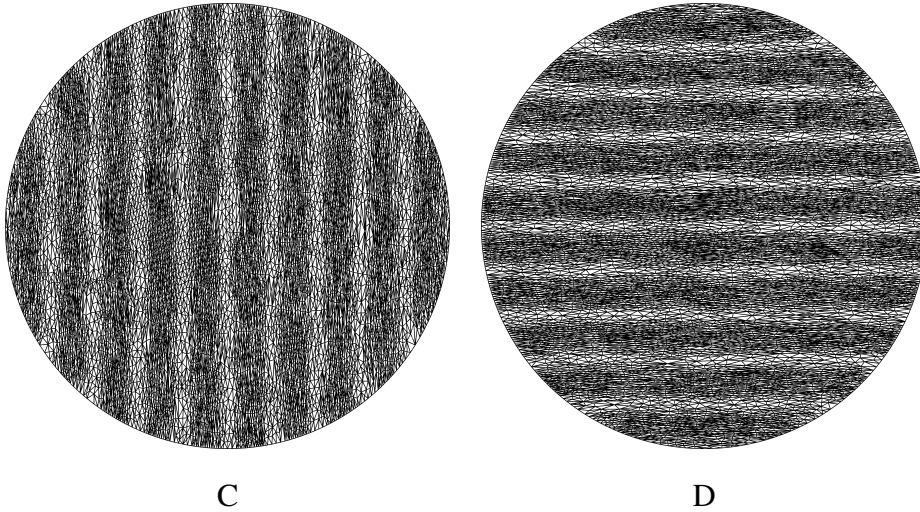


Fig. 5. Anisotropic meshes used to test for imbalance injection by mesh-to-mesh interpolation. There is no relationship between meshes C and D, other than that they cover the same domain.

meshes C and D in figure 5, with a layer thickness initialised to random values in the interior and a value of zero on the boundary. The velocity field was initialised to be in discrete geostrophic balance with this layer thickness. The model was integrated as before, with interpolations backwards and forwards between two two meshes at 10 timestep

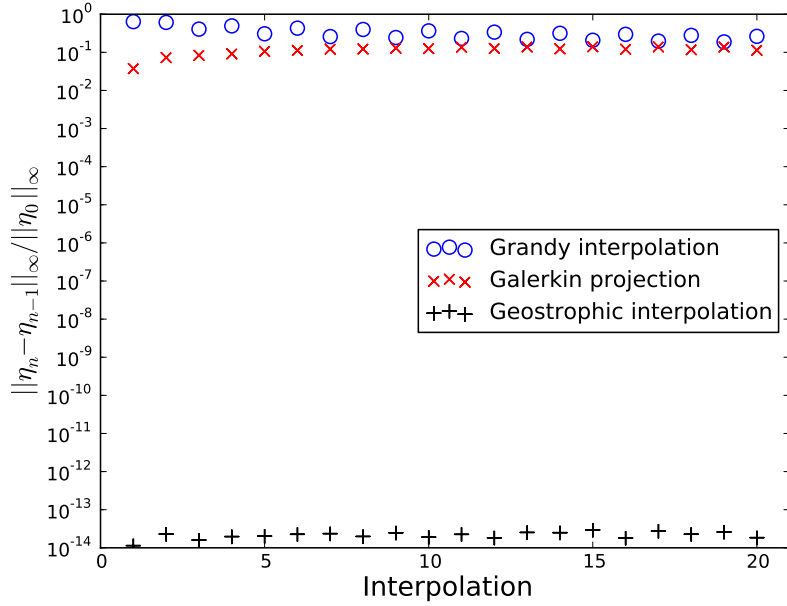


Fig. 6. The maximum change in layer thickness between interpolations backwards and forwards between the anisotropic meshes C and D in figure 5.

intervals for 4 interpolations, using the geostrophic balance preserving interpolant. The maximum change in layer thickness between interpolations was $\lesssim 10^{-12}$, and hence the solution was observed to be steady to within double precision round-off error.

3.2 Nearly balanced states

The Gaussian layer thickness profile in figure 2 had a perturbation applied of the form:

$$\Delta\tilde{\eta} = \frac{1}{10}X\tilde{\eta}, \quad (19)$$

where X is some point-wise random value in the range $\{0 - 1\}$. This perturbation was smoothed using a Helmholtz smoother with a characteristic length scale of $D/8$ to produce the layer thickness perturbation shown in figure 7. The velocity field was initialised to be in discrete geostrophic balance with the unperturbed layer thickness, thereby generating a nearly balanced state.

The system was integrated as before, with interpolations backwards and forwards between the pseudo-isotropic meshes A and B in figure 1 at 10 timestep intervals. One can

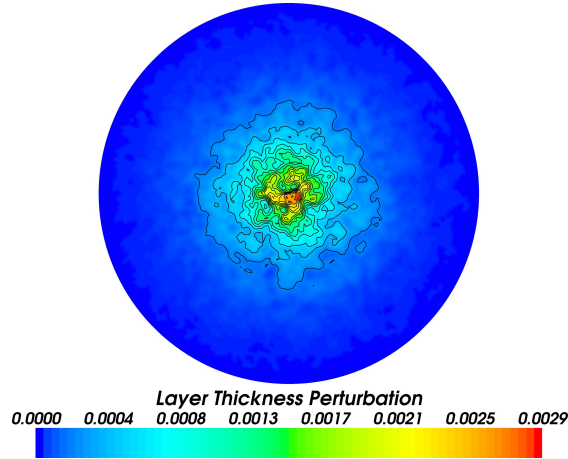


Fig. 7. Perturbation applied to the layer thickness in figure 2 to test for imbalance injection by interpolation of a nearly balanced state.

define an “imbalanced layer thickness”:

$$\tilde{\eta}_{imbal} := \tilde{\eta} - \frac{1}{g}\Phi, \quad (20)$$

where Φ is the scalar potential computed from the Helmholtz decomposition of the Coriolis acceleration. The final imbalanced layer thickness is shown for Galerkin projection and the geostrophic balance preserving interpolant in figure 8. When using Galerkin projection imbalance is observed to be injected near the layer thickness maximum. This additional imbalance dominates over the original layer thickness perturbation after 20 interpolations. When using the geostrophic balance preserving interpolant propagation of the original layer thickness perturbation is observed, with no significant pollution introduced by the interpolation.

Defining a “balanced velocity” $\tilde{\mathbf{u}}_{bal}$ where:

$$fL\tilde{\mathbf{u}}_{bal} := -gC\tilde{\eta}, \quad (21)$$

and an “imbalanced velocity” $\tilde{\mathbf{u}}_{imbal}$:

$$\tilde{\mathbf{u}}_{imbal} := \tilde{\mathbf{u}} - \tilde{\mathbf{u}}_{bal}, \quad (22)$$

allows one to compute an imbalanced kinetic energy:

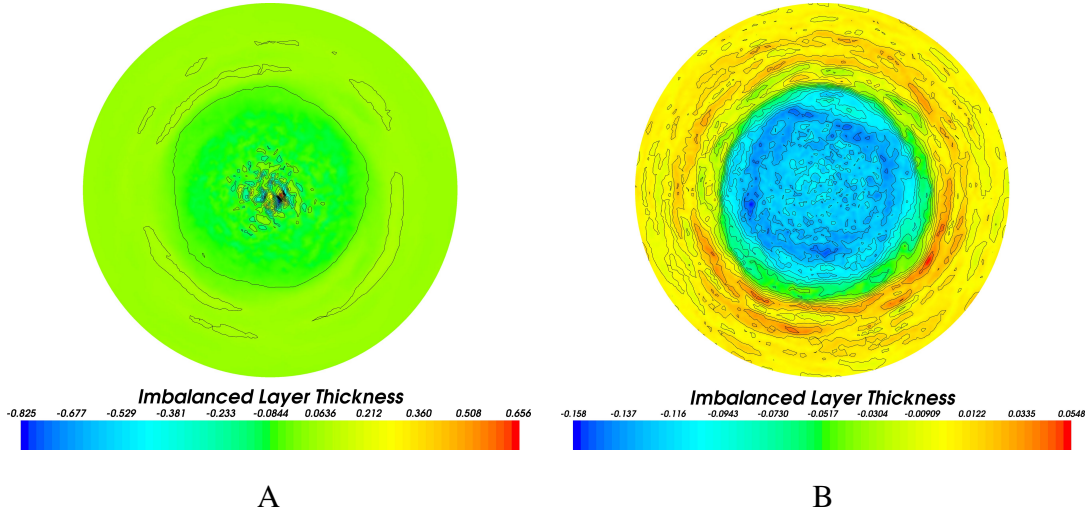


Fig. 8. The final imbalanced layer thickness, computed as the difference between the simulation layer thickness and the scaled scalar potential from the Helmholtz decomposition of the Coriolis acceleration. A: Galerkin projection. B: Helmholtz decomposed geostrophic balance preserving interpolation.

$$\begin{aligned}
 T_{imbal} &= \frac{1}{2} \|\tilde{\mathbf{u}}_{imbal}\|_{L^2}^2 \\
 &= \frac{1}{2} \left\| \tilde{\mathbf{u}} + \frac{g}{f} L^{-1} C \tilde{\eta} \right\|_{L^2}^2.
 \end{aligned} \tag{23}$$

The imbalanced kinetic energies when using Galerkin projection and the geostrophic balance preserving interpolant are shown in figure 9. When using Galerkin projection the imbalanced kinetic energy is observed to increase by up to a factor of 70 in an interpolation, with the imbalanced kinetic energy peaking at 150 times its initial value. When using the geostrophic balance preserving interpolant the imbalanced kinetic energy is observed to increase by at most a factor 1.02 in an interpolation, and the imbalanced kinetic energy never exceeds its initial value.

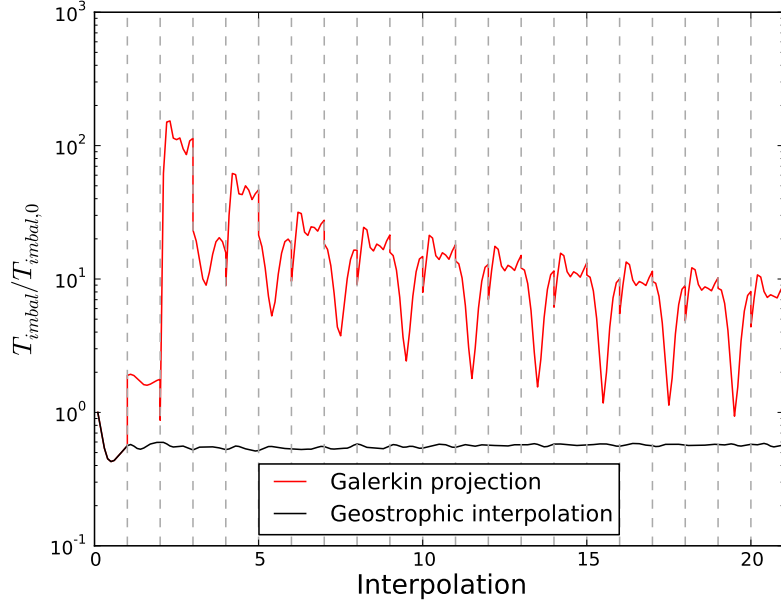


Fig. 9. The imbalanced kinetic energy, normalised by the initial imbalanced kinetic energy, for the nearly balanced interpolation test. When using Galerkin projection (upper line) large increases in the imbalanced kinetic energy are observed after interpolation, with these increases dominating over the original imbalanced kinetic energy. When using the geostrophic balance preserving interpolant (lower line) imbalanced kinetic energy injection is significantly reduced.

3.3 Kelvin wave

The interpolant was tested for a Kelvin wave, configured as in in Ham et al. (2005); Cotter et al. (2009b) with an initial condition:

$$\eta(r, \theta) = \exp\left(\frac{r - r_0}{Ro}\right) \cos \theta, \quad (24a)$$

$$u_\theta(r, \theta) = \frac{1}{Fr} \exp\left(\frac{r - r_0}{Ro}\right) \cos \theta, \quad (24b)$$

$$u_r = 0, \quad (24c)$$

for $Ro = 10$ and $Fr = 1$ in a circular domain of radius r_0 . The Kelvin wave is geostrophically balanced in the direction normal to the boundary and imbalanced in the tangential direction. The model was integrated with a timestep of $2\pi \times 10^{-4}(D/U)$ for a total simulated time of $2\pi(D/U)$, corresponding to the time taken for a single Kelvin wave to perform a circuit of the domain in the limit of large r_0 . Two meshes of quasi-uniform

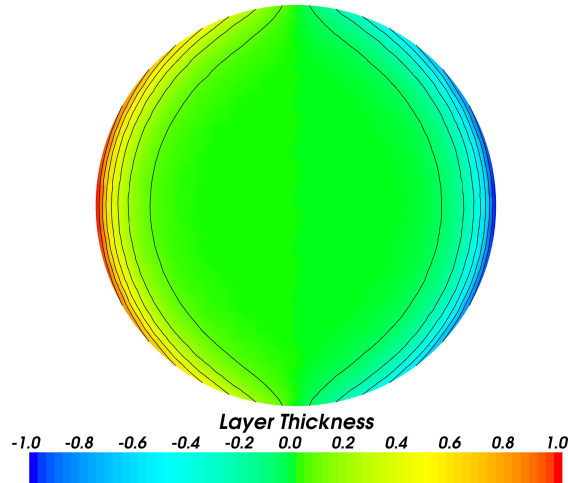


Fig. 10. Initial layer thickness used for the Kelvin wave test at $Ro = 10$, $Fr = 1$.

resolution with 1473 and 1461 nodes respectively were created using gmsh (Geuzaine and Remacle, 2009) and the ani2d mesh optimisation library (Vasilevskii and Lipnikov, 1999; Agouzal et al., 1999), and the solution interpolated backwards and forwards between these meshes at 10 timestep intervals.

The initial layer thickness is shown in figure 10, and the Helmholtz decomposition of the initial Coriolis acceleration in figure 11. The final solutions when using Galerkin projection and the geostrophic balance preserving interpolant are shown in figure 12. Relatively little difference is observed in the final layer thickness field between these simulations. However, when using Galerkin projection, noise is observed in the velocity divergence field, originating at the boundary. This noise is significantly reduced when using the geostrophic balance preserving interpolant.

A discretisation of the linearised shallow-water equations conserves energy if the layer thickness gradient matrix is, after multiplication by some diagonal matrix, equal to the transpose of the velocity divergence matrix (Ham et al., 2007), and if the implicit midpoint rule is used for timestepping (Leimkuhler and Reich, 2004). Hence the $P_{1DG}P_2$ spatial discretisation of the linearised shallow-water equations as presented here conserves the total energy. The kinetic, potential, and total energy of the system when using Galerkin projection, the geostrophic balance preserving interpolant, and when using a single fixed computational mesh, are shown in figure 13. The fixed mesh simulation is observed to conserve the total energy to within one part in 10^4 , with the relatively high error attributed to the tolerances used for the linear solvers. The use of direct solvers, combined with more precision robust calculation of the energy diagnostics, is expected to decrease this error. When interpolating between meshes using Galerkin projection a systematic dissipation of both kinetic and potential energy is observed, leading to a

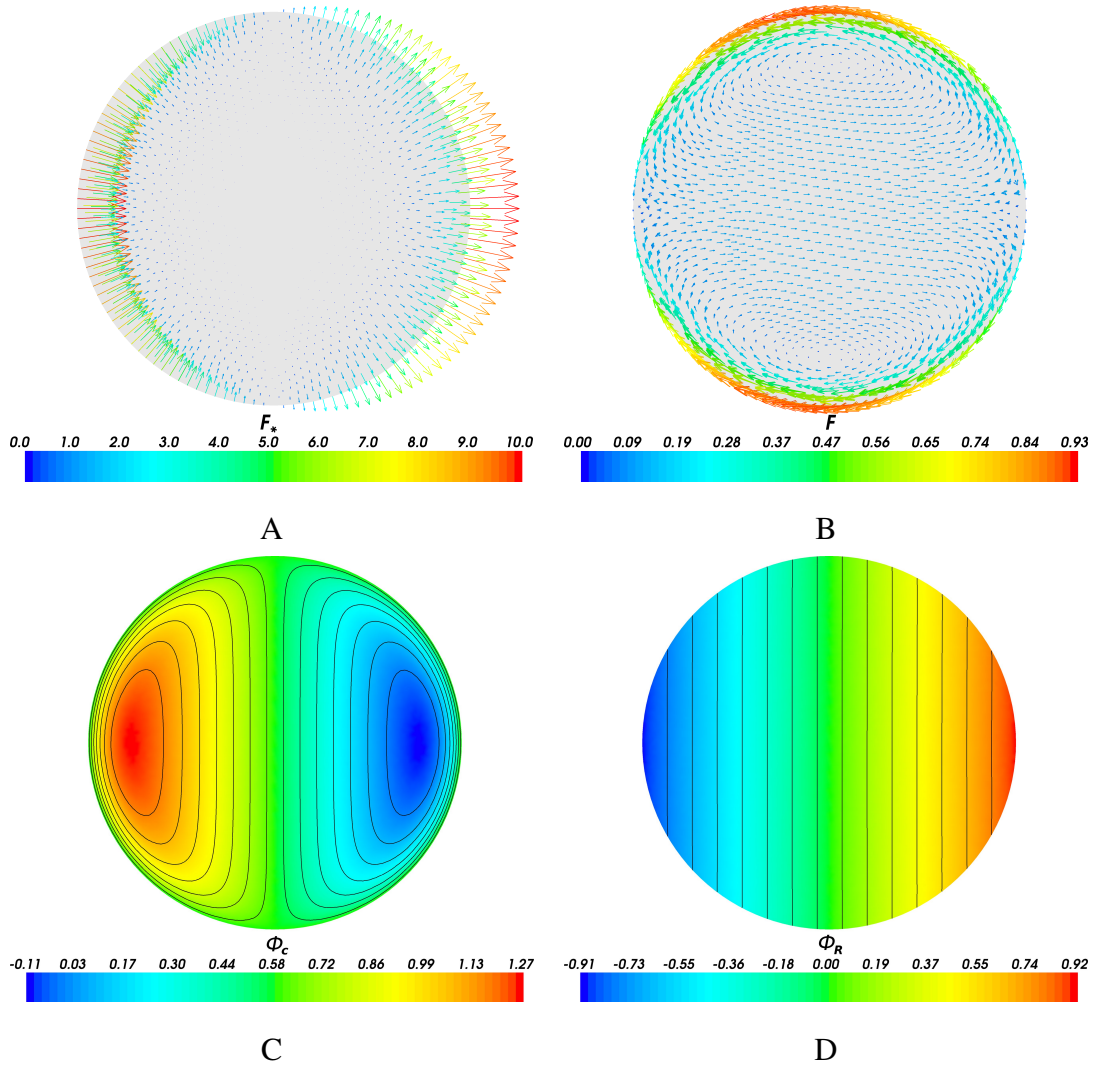


Fig. 11. Helmholtz decomposition of initial Coriolis acceleration for the Kelvin wave test at $Ro = 10$, $Fr = 1$. A: Coriolis acceleration, F_* . B: Non-divergent residual, F . C: Scalar potential with a constant boundary value, Φ_C . D: Scalar potential residual, Φ_R .

decrease in the total system energy of 1.3% after 1000 interpolations, at the end of the simulation. When using the geostrophic balance preserving interpolant a slight increase the potential energy is observed, leading to an increase in the total system energy of 0.11% after 1000 interpolations. While the geostrophic balance preserving interpolant is not energy conserving, the change in system energy is, for this test, more than an order of magnitude smaller than that observed when applying Galerkin projection.

In further testing it was found that highly anisotropic elements intersecting the domain boundary led to very poor results when using the geostrophic balance preserving in-

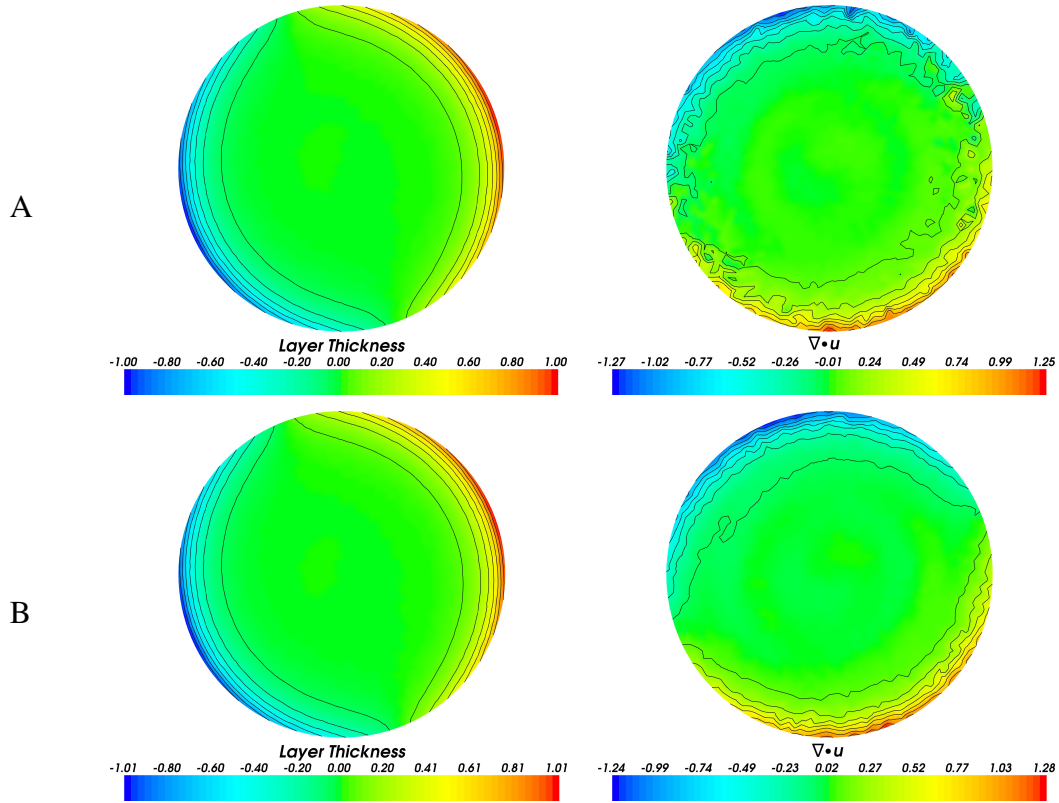


Fig. 12. The final solution of the Kelvin wave test at $Ro = 10$, $Fr = 1$ Left: Final layer thickness. Right: Final velocity divergence, $M_2^{-1}C^T\tilde{\mathbf{u}}$. A: Galerkin projection. B: Helmholtz decomposed geostrophic balance preserving interpolation.

terpolant. This is likely due to significant interpolation errors in the projection of Φ in this region, possibly as a result of the Dirichlet boundary condition for Φ_c in the mesh-to-mesh Galerkin projection, which pollutes the interpolated Coriolis acceleration. This problem was solved by imposing constraints on the maximum element size for elements directly on the boundary.

3.4 Accuracy

Since the geostrophic balance preserving interpolant is composed of a Galerkin discretisation of the Helmholtz decomposition of the Coriolis acceleration followed by a donor-to-target Galerkin projection of the decomposition, when using the $P_{1DG}P_2$ element pair the interpolant is expected to be second order accurate for velocity and third order accurate for layer thickness.

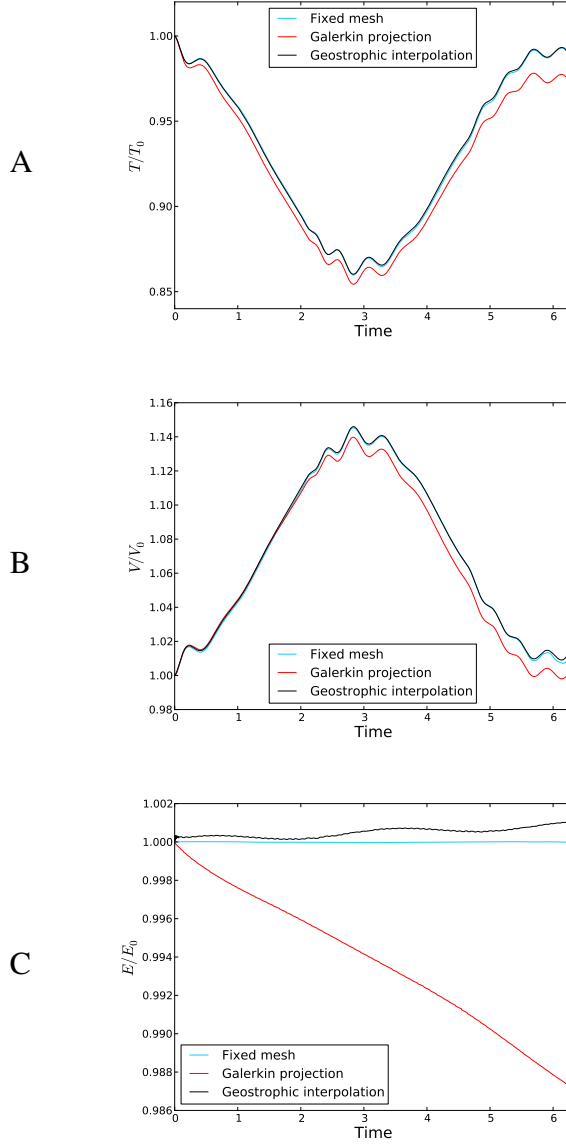


Fig. 13. The energy of the Kelvin wave test when interpolating between meshes using Galerkin projection and the geostrophic balance preserving interpolant, and when using a single fixed computational mesh. A: Kinetic energy. B: Potential energy. C: Total energy.

A series of structured triangular mesh pairs for a 2D unit square $-0.5 \leq x \leq 0.5$ and $-0.5 \leq y \leq 0.5$ were generated with resolutions in the x - and y -directions as given in table 1. A layer thickness of the form:

$$\eta = \sin(2.5\pi x) \sin(2.5\pi y), \quad (25)$$

Donor mesh resolution ($x \times y$)	Target mesh resolution($x \times y$)
24×26	26×24
32×35	35×32
48×52	52×48
64×70	70×64
96×105	105×96
128×130	130×128
192×215	215×196

Table 1

Mesh resolutions used for the geostrophic balance preserving interpolant convergence test. A mesh resolution of $N \times M$ denotes a division in the x -direction into N sections, a division in the y -direction into M sections, and the division of each resulting quadrilateral into two triangles.

and a velocity of the form:

$$\mathbf{u} = -\hat{\mathbf{z}} \times \nabla \eta + \sin(0.5x)\hat{\mathbf{x}} + \sin(0.5x)\hat{\mathbf{y}}, \quad (26)$$

were interpolated between the meshes in each pair using the geostrophic balance preserving interpolant. The first term in (3.4) corresponds to a flow that is, for $f = -1$, $g = 1$ and $H = 1$, in geostrophic balance with the layer thickness (3.4). The remaining terms correspond to a flow that cannot be balanced by any layer thickness. In order to test for additional error introduced by the scalar potential Φ and layer thickness decomposition, as per equation (15), tests were conducted for a doubly periodic and for a bounded domain. The L_2 errors $\|\tilde{\eta}_B - \tilde{\eta}_A\|_{L^2}$, $\|\tilde{u}_{x,B} - \tilde{u}_{x,A}\|_{L^2}$ and $\|\tilde{u}_{y,B} - \tilde{u}_{y,A}\|_{L^2}$, were computed explicitly via supermesh construction, as described in Farrell (2009). For comparison the fields were also projected using Galerkin projection, giving a measure of the quality of the geostrophic balance preserving interpolant relative to the projection that is optimal in the L_2 norm.

The resulting errors are shown for the doubly periodic domain in figure 14 and for the bounded domain in figure 15. The geostrophic balance preserving interpolant is observed to be second order accurate for velocity and third order accurate for layer thickness, as expected. For the doubly periodic domain the average L_2 norm error for the geostrophic balance preserving interpolant is observed to be 1.37 times the optimal value for velocity, and (since no layer thickness decomposition is applied in this case)

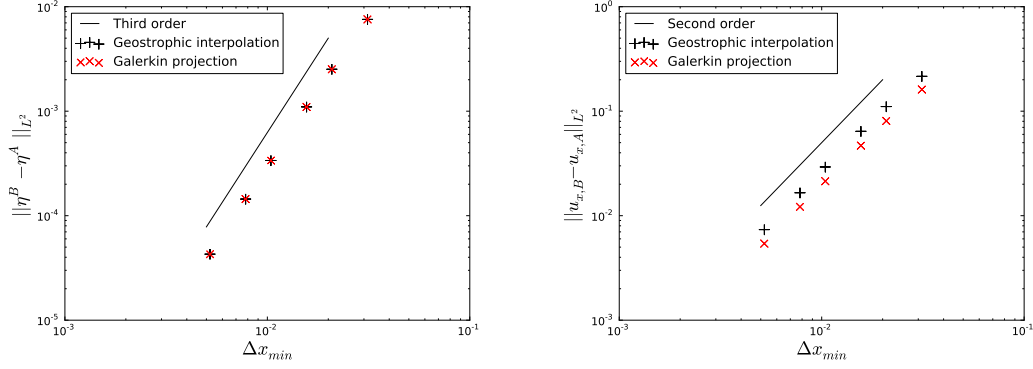


Fig. 14. Convergence test for the geostrophic balance preserving interpolant in a doubly periodic domain, with Galerkin projection for comparison. Left: L_2 error in the layer thickness. Right: L_2 error in the x -component of velocity. The error in the y -component of velocity is similar.

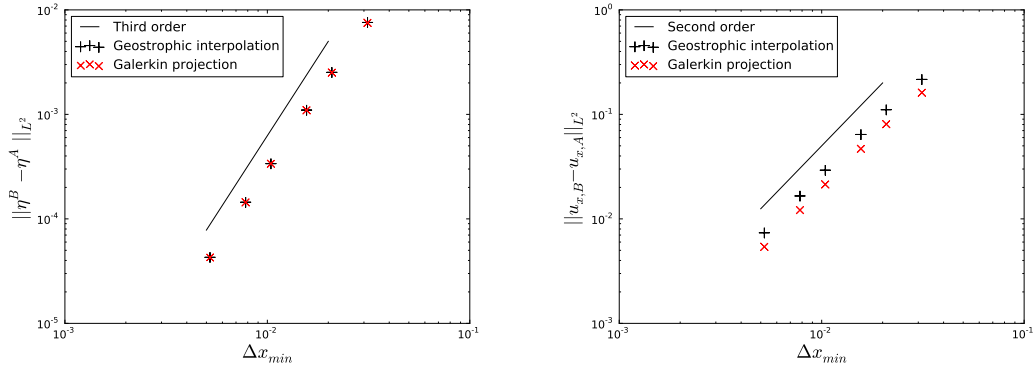


Fig. 15. Convergence test for the geostrophic balance preserving interpolant in a bounded domain, with Galerkin projection for comparison. Left: L_2 error in the layer thickness. Right: L_2 error in the x -component of velocity. The error in the y -component of velocity is similar.

optimal for layer thickness. For the bounded domain the error in velocity is not significantly changed, and the error in layer thickness is increased to 1.005 times the optimal value, indicating that the decomposition of the scalar potential Φ_A and layer thickness $\tilde{\eta}_A$ introduces only a small additional error. For comparison, in Farrell (2009) collocation is found to give, for a field $\sin x + \cos x$, an L_2 error that is $\sim 2 - 2.5$ times the optimal value for piecewise linear elements, and ~ 1.1 times the optimal value for piecewise quadratic elements.

4 Conclusions

We have presented an interpolation method that, when applied to the $P_{1DG}P_2$ discretisation of the linearised shallow-water equations on an f -plane, guarantees that steady and geostrophically balanced states on the donor mesh remain steady and geostrophically balanced after interpolation onto an arbitrary target mesh. We have stress tested this balance preserving property with highly anisotropic meshes and randomly initialised balanced states (constrained to satisfy appropriate boundary conditions). We have further demonstrated the utility of this interpolant for nearly balanced dynamics, and quantified its accuracy in the L_2 norm.

A shortcoming of this approach, at least in the form presented, is that it does not conserve energy. The Helmholtz decomposed interpolation of Coriolis acceleration does not conserve kinetic energy or potential energy. Despite this, the change in energy when using the geostrophic balance preserving interpolant was found to be more than an order of magnitude smaller than the energy dissipation when using Galerkin projection. In addition to this, the interpolant does not locally conserve potential vorticity. Geophysical flows are only in geostrophic balance to leading order, and a lack of potential vorticity conservation could, when non-linear advection is included in the fundamental equations, lead to higher order balance loss. Potential vorticity decompositions could be considered where such a conservation is desired (Staquet and Riley, 1989; Holopainen and Kaurola, 1991; McIntyre and Norton, 2000), although the benefit of such an approach, bearing in mind that discretisations of the non-linear shallow-water equations are not generally potential vorticity conserving, may be somewhat limited compared to the benefit of leading order balance preservation.

The method has a natural extension to Navier-Stokes. For incompressible Navier-Stokes any forcing that can be represented as the gradient of a scalar field must be filtered by the pressure gradient, and hence the interpolation of the Helmholtz decomposition of the Coriolis acceleration is a balance preserving interpolant. Future work will concentrate on the implementation of geostrophic balance preserving interpolation as part of the Imperial College Ocean Model - an unstructured dynamic mesh adaptive ocean model. In particular, we will investigate accurate preservation of geostrophic balance when using velocity-pressure element pairs that do not satisfy optimal balance properties, and the integration of methods used for accurate balance representation for such element pairs (Ford et al., 2004a,b; Piggott et al., 2006, 2008b; Fang et al., 2009) into a balance preserving interpolant. We will test how these can be used to propagate accurate balance representation through arbitrary mesh adapts for meshes that are fully unstructured in all three dimensions.

5 Acknowledgements

The authors wish to acknowledge support from the UK Natural Environment Research Council (grants NE/C52101X/1, NE/C51829X/1 and NE/H527032/1). The authors would also like to thank Prof. David P. Marshall and Dr. Hilary Weller for their comments and suggestions in preparing this article.

References

- Agouzal, A., Lipnikov, K., Vassilevski, Y., 1999. Adaptive generation of quasi-optimal tetrahedral meshes. *East west journal of numerical mathematics* 7 (4), 223–244.
- Balay, S., Buschelman, K., Eijkhout, V., Gropp, W. D., Kaushik, D., Knepley, M. G., McInnes, L. C., Smith, B. F., Zhang, H., 2008. PETSc Users Manual. Argonne National Laboratory, anl-95/11 - revision 3.0.0 Edition.
- Balay, S., Buschelman, K., Gropp, W. D., Kaushik, D., Knepley, M. G., McInnes, L. C., Smith, B. F., Zhang, H., 2009. PETSc Web page. <http://www.mcs.anl.gov/petsc>.
- Balay, S., Gropp, W. D., McInnes, L. C., Smith, B. F., 1997. Efficient management of parallelism in object oriented numerical software libraries. In: Arge, E., Bruaset, A. M., Langtangen, H. P. (Eds.), *Modern Software Tools in Scientific Computing*. Birkhäuser Press, pp. 163–202.
- Chorin, A. J., 1967. A numerical method for solving incompressible viscous flow problems. *Journal of Computational Physics* 2 (1), 12–26.
- Comblen, R., Legrand, S., Deleersnijder, E., Legat, V., 2009. A finite element method for solving the shallow water equations on the sphere. *Ocean Modelling* 28 (1-3), 12–23.
- Cotter, C. J., Ham, D. A., Pain, C. C., 2009a. A mixed discontinuous/continuous finite element pair for shallow-water ocean modelling. *Ocean Modelling* 26 (1-2), 86–90.
- Cotter, C. J., Ham, D. A., Pain, C. C., Reich, S., 2009b. LBB stability of a mixed Galerkin finite element pair for fluid flow simulations. *Journal of Computational Physics* 228 (2), 336–348.
- Crank, J., Nicolson, P., 1947. A practical method for numerical evaluation of solutions of partial differential equations of the heat-conduction type. *Proc. Cambr. Phil. Soc* 43, 50–67.
- Fang, F., Pain, C. C., Navon, I. M., Gorman, G. J., Piggott, M. D., Allison, P. A., Farrell, P. E., Goddard, A. J. H., 2009. A POD reduced order unstructured mesh ocean modelling method for moderate Reynolds number flows. *Ocean Modelling* 28 (1-3), 127–136.
- Farrell, P. E., 2009. Galerkin projection of discrete fields via supermesh construction. Ph.D. thesis, Imperial College London.

- Farrell, P. E., Piggott, M. D., Pain, C. C., Gorman, G. J., Wilson, C. R., 2009. Conservative interpolation between unstructured meshes via supermesh construction. *Computer Methods in Applied Mechanics and Engineering* 198 (33-36), 2632–2642.
- Ford, R., Pain, C. C., Piggott, M. D., Goddard, A. J. H., de Oliveira, C. R. E., Umpleby, A. P., 2004a. A nonhydrostatic finite-element model for three-dimensional stratified oceanic flows. Part I: Model Formulation. *Monthly Weather Review* 132 (12), 2816–2831.
- Ford, R., Pain, C. C., Piggott, M. D., Goddard, A. J. H., de Oliveira, C. R. E., Umpleby, A. P., 2004b. A nonhydrostatic finite-element model for three-dimensional stratified oceanic flows. Part II: Model validation. *Monthly weather review* 132 (12), 2832–2844.
- Geuzaine, C., Remacle, J. F., 2009. Gmsh: a three-dimensional finite element mesh generator with built-in pre-and post-processing facilities. *International Journal for Numerical Methods in Engineering* 79 (11), 1309–1331.
- Grandy, J., 1999. Conservative remapping and region overlays by intersecting arbitrary polyhedra. *Journal of Computational Physics* 148 (2), 433–466.
- Gresho, P. M., 1990. On the theory of semi-implicit projection methods for viscous incompressible flow and its implementation via a finite element method that also introduces a nearly consistent mass matrix. Part 1: Theory. *International Journal for Numerical Methods in Fluids* 11 (5), 587–620.
- Ham, D. A., Kramer, S. C., Stelling, G. S., Pietrzak, J., 2007. The symmetry and stability of unstructured mesh C-grid shallow water models under the influence of Coriolis. *Ocean Modelling* 16 (1-2), 47–60.
- Ham, D. A., Pietrzak, J., Stelling, G. S., 2005. A scalable unstructured grid 3-dimensional finite volume model for the shallow water equations. *Ocean Modelling* 10 (1-2), 153–169.
- Holopainen, E., Kaurola, J., 1991. Decomposing the atmospheric flow using potential vorticity framework. *Journal of the Atmospheric Sciences* 48, 2614–2625.
- Ladyzhenskaya, O. A., 1969. *The mathematical theory of viscous incompressible flow*. New York, 10.
- Le Roux, D. Y., Staniforth, A., Lin, C. A., 1998. Finite elements for shallow-water equation ocean models. *Monthly Weather Review* 126 (7), 1931–1951.
- Leimkuhler, B., Reich, S., 2004. *Simulating Hamiltonian dynamics*. Cambridge Univ Pr.
- McIntyre, M. E., Norton, W. A., 2000. Potential vorticity inversion on a hemisphere. *Journal of the Atmospheric Sciences* 57 (9), 1214–1235.
- Munday, D. R., Marshall, D. P., Piggott, M. D., 2010. Idealised flow past an island in a dynamically adaptive finite element model. *Ocean Dynamics*, in press.
- Pain, C. C., Piggott, M. D., Goddard, A. J. H., Fang, F., Gorman, G. J., Marshall, D. P., Eaton, M. D., Power, P. W., de Oliveira, C. R. E., 2005. Three-dimensional unstructured mesh ocean modelling. *Ocean Modelling* 10 (1-2), 5–33.

- Pain, C. C., Umpleby, A. P., De Oliveira, C. R. E., Goddard, A. J. H., 2001. Tetrahedral mesh optimisation and adaptivity for steady-state and transient finite element calculations. *Computer Methods in Applied Mechanics and Engineering* 190 (29-30), 3771–3796.
- Piggott, M. D., Gorman, G. J., Pain, C. C., Allison, P. A., Candy, A. S., Martin, B. T., Wells, M. R., 2008a. A new computational framework for multi-scale ocean modelling based on adapting unstructured meshes. *International Journal for Numerical Methods in Fluids* 56 (8), 1003.
- Piggott, M. D., Pain, C. C., Gorman, G. J., Marshall, D. P., Killworth, P. D., 2008b. Unstructured adaptive meshes for ocean modeling.
- Piggott, M. D., Pain, C. C., Gorman, G. J., Power, P. W., Goddard, A. J. H., 2006. h, r, and hr adaptivity with applications in numerical ocean modelling. *Ocean Modelling* 10 (1-2), 95–113.
- St-Cyr, A., Jablonowski, C., Dennis, J. M., Tufo, H. M., Thomas, S. J., 2008. A comparison of two shallow water models with non-conforming adaptive grids. *Monthly Weather Review* 136 (6), 1898.
- Staquet, C., Riley, J. J., 1989. On the velocity field associated with potential vorticity. *Dynamics of Atmospheres and Oceans* 14, 93–123.
- Temam, R., 1968. Une méthode d'approximation de la solution des équations de Navier-Stokes. *Bull. Soc. Math. France* 98, 115–152.
- Vasilevskii, Y. V., Lipnikov, K. N., 1999. An adaptive algorithm for quasioptimal mesh generation. *Computational mathematics and mathematical physics* 39 (9), 1468–1486.
- Weyl, H., 1940. The method of orthogonal projection in potential theory. *Duke Mathematical Journal* 7 (1), 411–444.